Talanta 107 (2013) 239–247

Contents lists available at SciVerse ScienceDirect

Talanta

journal homepage: www.elsevier.com/locate/talanta

Flexible sensor based on carbon nanofibers with multifunctional sensing features

O. Monereo [a,*], S. Claramunt [a], M. Martínez de Marigorta [b], M. Boix [a], R. Leghrib [a], J.D. Prades [a], A. Cornet [a], P. Merino [c], C. Merino [c], A. Cirera [a]

[a] MIND/IN2UB Electronics Department, Universitat de Barcelona, c/Martí i Franquès 1, Planta 2, Barcelona 08028, Spain
[b] WorldSensing S.L.N.E., Barcelona, Spain
[c] Grupo Antolin Ingenieria S.A., Burgos, Spain

ARTICLE INFO

Article history:
Received 24 May 2012
Received in revised form
4 January 2013
Accepted 11 January 2013
Available online 21 January 2013

Keywords:
Inkjet
Gas sensor
Room temperature
Carbon nanofibers
Flexible electronics
Mutifunctional

ABSTRACT

Herein, we present the fabrication and characterization of a flexible gas sensor based on carbon nanofibers. The sensing device is composed of interdigitated silver electrodes deposited by inkjet printing on Kapton substrates, subsequently coated with carbon nanofibers as sensing element. Gas sensing response to CO, NH_3 and humidity has been characterized in detail. Thermal, mechanical and electromagnetic radiation effects have also been studied and discussed from the point of view of the cross-sensitivity. The obtained results open the door for a new generation of flexible sensors with multifunctional sensing features, which are producible with scalable techniques based on low cost nanomaterials.

1. Introduction

The development of new smart sensor networks for the monitoring of environmental parameters for comfort, health, safety, and security purposes demands for new solid state gas sensors with better performances. Up to now, considerable effort has been devoted to improve operating parameters such as sensitivity, selectivity, and reliability of the sensors.

For on-site monitoring applications, devices with low power consumption, low-cost, high efficiency, and portability are highly desirable. Some demonstrations of such devices are under investigation and involve the development of sensors based on flexible substrates, partially owing to the increasing proliferation of handheld, portable consumer electronics [1,2]. Fabrication of flexible sensor platforms has been investigated and provides a wide range of applications, featuring low cost, light weight and mechanical flexibility [3]. Devices supported on plastic foils are required to realize intelligent RFID tags for environmental monitoring, flexible active matrix displays, electronics skins, flexible solar cells and disposable printed electronics [4–7], and represent a cost effective alternative to expensive silicon technology, which could eventually find application in wearable systems, smart buildings, and in the logistics of perishable products. The pending challenges are not only their manufacture, but also the stability of their mechanical, electrical and gas sensing properties.

Printed electronics are becoming a more and more mature technology every day, and new kinds of products are expected in the near future. Besides, a strong potential for cost-effective production with a reduced infrastructure, the benefits of printing devices on plastic foil include their potential to be lightweight, foldable/rollable, transparent, thin, conformal, wearable, and produced on a large scale. In the last decade, inkjet printing has grown to a major topic in scientific research. Today, inkjet printing is a competitive method to conventional printing techniques such as photolithography for the production of electronic devices [8,9]. Furthermore, inkjet printing is compatible with many types of substrates, non-contact and no-mask patterning, low temperature processing, and no requirement for vacuum [10,11].

There are a limited number of publications on gas sensors on plastic/flexible foils, but this number is growing up. Most of these works used substrates as polyethylene-terephthalate (PET), polyethylene naphthalate (PEN) and polyimide (PI). As a matter of fact, Torsi et al. fabricated a thin-film transistor gas sensor, comprising an outermost layer with built-in enantioselective properties that exhibits a field-effect amplified sensitivity that

* Corresponding author. Tel.: +34 93 4034804; fax: +34 93 4021148.
E-mail address: omonereo@el.ub.edu (O. Monereo).

0039-9140/$ - see front matter © 2013 Elsevier B.V. All rights reserved.
http://dx.doi.org/10.1016/j.talanta.2013.01.022

enables differential detection of optical isomers in the range of tens-of ppm [12]. Other works reported on the detection at room temperature of volatile organic compounds, sub-ppm levels of ammonia and hydrogen sulphide, and ppm levels of nitrogen oxides, some of which using printing technologies (e.g., inkjet printing) to deposit gas-sensitive conducting polymers and silver electrodes [13–18]. However, the sensing performance achieved was poor and requires further development to meet the sensing performances and reliability demanded by the market, as discussed by Subramanian et al. [19].

In the present paper, a new approach for developing flexible gas sensors based on carbon nanofibers is presented. Our aim is to achieve an easy, fast and inexpensive methodology to produce low power consumption gas alarms integrable in textile or other non-usual localizations. For this purpose, Kapton was used as flexible substrate, due to its physical and chemical advantages, on which interdigited silver electrodes were deposited by inkjet printing methods. These were later coated with carbon nanofibers by means of spray technique [20,21]. Carbon materials, which are well-known by rendering significant responses to gases even at room temperature, permit to lower the power consumption of the sensor. In order to evaluate the performance of the sensors developed, their gas sensing properties to CO, NH_3 and humidity at room temperature as well as the effects of thermal, mechanical and electromagnetic radiation stimuli were thoroughly studied.

2. Experimental

2.1. Sensor fabrication

Kapton (polyimide) commercially available from DuPont, with thickness of 50 μm, was chosen as flexible substrate. It has a typical dielectric strength of 240 kV/mm [22], which makes it suitable for electronic circuitry. The key advantages of this polyimide compared to other polymers is that it can be heated up to 350 °C, as a second order glass transition occurs between 360 °C and 410 °C [22]. Therefore, moderate thermal treatments of the materials can be performed even after being deposited. From the mechanical point of view, it also displays good flexibility and resistance [22]. Another advantage, which is common in most of the polymers, is its low mass, which makes it more resistant to vibration and sudden mechanical energy transfers. This makes it appropriate for future devices more reliable in environments, such as automotive applications, where mechanical resistance is a special concern. All these points justify the election of Kapton as flexible substrate used in this present work.

The fabrication of the metal contacts was made by inkjet deposition of commercial silver ink U5603 (SunTronic Inc., USA) with 20 wt% of silver. An automatic controlled inkjet system with inkjet dispenser Xenjet 4000 (Xennia Technology Ltd., UK). The cartridge was an Omnidot 760 (Xaar, Ltd., UK), based on piezo-resistive technology to eject the ink. Once the ink was deposited, the circuits were heated to 200 °C for 20 min to stabilize the silver and evaporate the ink's solvent. Several designs were conceived and implemented: ten conductive bars (with widths of 0.7 mm for each bar and pitch of 1 mm between them designed following the specifications of a commercial FFC/FPC connector), two conductive bars (2 mm wide and pitch of 2.54 mm designed for a clincher commercial socket), 4-probes circuit optimized for van der Pauw measurements [23,24], and interdigited configuration for sensor testing. This last one included several alternative variations: terminations for FFC/FPC connector and square pads for probe station testing. Examples of interdigited printed circuits used in this work are showed in the Supplementary materials.

2.2. Material deposition

Carbon nanofibers, supplied by Grupo Antolín, having a diameter between 20 and 80 nm and lengths of more than 30 μm, were first dispersed in 2-propanol and then deposited over interdigited silver electrodes using spray technique [20,21]. The deposited film was homogenous with a thickness of hundreds of nanometers except for the edges, which displayed a linearly growing profile. Two kinds of nanofibers were tested, one with a graphitization of ~70% (GANF) and one with ~100%, (GANFG), further details of these nanofibers have been given elsewhere [25].

2.3. Characterization

A series of experiments were designed and performed in order to evaluate the electrical, thermal, mechanical and sensing properties of the devices based on GANF and GANFG nanofibers. The response of the sensor to gas and by radiation was defined as the difference between the resistance when there is a change of the physical measured property (R), and the initial resistance value (R_0) normalized to R_0.

$$\text{Response}(\%) = \frac{R - R_0}{R_0} \times 100 = \frac{\Delta R}{R_0} \quad (1)$$

2.3.1. Electrical and thermal characterization

To evaluate the electrical properties of the samples, different kinds of measurement were conducted using a sourcemeter unit SMU 2400 (Kethley Ltd., USA) and a multimeter 3458A (Agilent Inc., USA). All connected to 4-probes station, which featured a temperature controller capable of setting the sample's temperature from room temperature (25 °C) up to 300 °C. Tungsten probe tips (72T-J3 from American Probe & Technologies Inc. USA, with straight shape and radius of 7 μm) were used to obtain a reliable and stable contact with the silver pads of the samples. All the temperature treatments shown below were carried out in ambient atmosphere. First of all, studies of the sheet resistance of the nanofibers were done using the van der Pauw method [23,24]. These resistance values were quite independent of the asymmetry between contacts of the thermoelectric contributions at each different metal-fiber interface.

Subsequently, in order to study the contribution of the contacts interface to the total resistance of the sample, measurements of the resistance of the fibers films at different interelectrode distances were conducted. The total resistance of the sample can be easily rationalized as a contribution from the two contacts and a contribution from the fibers. Therefore, we can write:

$$R_{\text{measured}-2P} \equiv R_{\text{sample}} + 2R_c \quad (2)$$

where $R_{\text{measured}-2p}$ is the experimental value of the total resistance (defined as R_{2P} since it is the resistance measured in 2-probes studies), R_{sample} is the intrinsic resistance value of the nanofibers film, and R_c is the resistance of each one of the contacts between the nanofibers and the silver electrodes. Since the R_{sample} is expected to be proportional to the distance between contacts l, then it is easy to determine R_c by extrapolating the value of the total resistance at distance zero from a series of $R_{\text{measured}-2p}$ values vs. l. The extrapolated point gives a direct measurement of the contribution of the contacts to the total value of measured resistance.

2.3.2. Gas testing

Sensing characterization was carried out in a gas test system conceived to characterize micro and nanodevices, which included a MGP-2 gas mixer (Gometrics S.L., Spain) and a 4200-SCS Semiconductor Characterization System equipped with 3 sourcemeter

units (Keithley Ltd., USA). A LabVIEW program controlled all these components.

Experiments were exclusively performed in a customized chamber (15 ml in volume) in which the gas flow was maintained constant at 200 ml/min. Accurate gaseous environments were provided by the mass flow controllers of the MGP2 system connected to calibrated bottles of dry synthetic air (SA, which contains 21% of O_2 diluted in 79% of N_2), CO (1000 ppm $\pm$1% in SA) and NH_3 (1000 ppm $\pm$1% in SA). The water vapour was introduced in the gas mixture bubbling dry synthetic air through a vase containing deionized water at room temperature (25 °C).

2.3.3. Mechanical characterization

Mechanical test were performed in order to check if the flexibility itself by bending can alter the signal of the sensor. To that end, a configuration of deflected beam was chosen (see more details below). An experimental setup formed by two suspended clamps fixed with micropositioners was built. The sample was connected to a board to extract the resistive signal using SMU 2400. This configuration allowed us to modulate the bending of the substrate.

The response is quantified by a parameter called the gauge factor g, defined as the difference of resistance change ($\Delta R = R - R_0$) produced by a strain ε normalized to the initial resistance R_0:

$$g = \frac{\Delta R}{R_0}\frac{1}{\varepsilon} \tag{3}$$

In order to evaluate the strain ε, a configuration of a symmetric deflected beam was chosen due to the fact that knowing the height y and the radius of curvature r of the flexible substrate the strain ε can be directly expressed as:

$$\varepsilon = \frac{y}{r} \tag{4}$$

Optical images were taken to evaluate y and r of the bend.

2.3.4. Effect of electromagnetic radiation

Two different energy ranges were studied in order to check the effect of electromagnetic radiation on carbon nanofibers: Ultra Violet radiation (UV) and visible light. For the measurements with UV, we used a Hamamatsu LC8 lamp (LC8 UV, Hamamatsu Photonics Inc., Japan) with a maximum power of 4500 mW/cm^2 at a wavelength of 365 nm, with dispersion from 220 nm to 580 nm. For the measurements with visible light, a solar simulator LS 150 SN 213 was used (Abet Technologies Inc., USA). To evaluate the power applied at the samples a UP19K-H powermeter (Gentec-EO, Inc., Canada) was used. Power intensity of 1140 mW/cm^2 was applied in all the experiments. In both cases, the samples were electrically probed by means of a Keithley 2400 sourcemeter unit (2400, Kethley Ltd., USA). In a semiconductor material under irradiation, the total carriers density can be expressed as the sum of the intrinsic one produced by thermal generation (n_0) and the carriers due to light generation Δn [26],

$$n = n_0 + \Delta n \tag{5}$$

This process produces a change in the resistance measured

$$\Delta R = R - R_0 = \frac{1}{\sigma}\frac{L}{A} - \frac{1}{q\mu n_0}\frac{L}{A} = \frac{1}{q\mu}\frac{L}{A}\left(\frac{-\Delta n}{n_0(n_0+\Delta n)}\right) \tag{6}$$

where R_0 is the initial resistance in dark and ΔR is the change in resistance produced by the impinging radiation, σ is the conductivity, L is the length of the material where the current goes through, A is the perpendicular area to the current, q is the charge of the electron and μ is the carriers charge mobility. This effect turns into a decrease in the resistance value R of the sample upon exposure to a pulse of radiation provided for photons which have sufficient energy to generate extra carriers. It can be demonstrated that, in moderate illumination conditions, the change in resistance is inversely proportional to the flux of light [27]. Therefore, pulses of different intensities should lead to different changes in the resistance, which makes this parameter suitable to detect and quantify the amount of impinging radiation. It can also be demonstrated that the number of generated carriers Δn can be expressed as

$$\Delta n = \frac{\eta\beta\tau}{\alpha^{-1}}\phi_{ph} \tag{7}$$

where η is the quantum efficiency, β is the fraction of photons not reflected at the surface, τ is the carrier lifetime, α is the absorption coefficient of the material and Φ_{ph} is the flux of photons [27]. Hence, the amount of carriers generated is directly proportional to the photon flux and the slope of this lineal law only depends on intrinsic properties of the material as analyzed in detail below. Finally, in order to study also the dynamic response of the signals, the response time (τ_{resp}) was defined as the time to change the resistance a 90% of the response upon exposure to a sudden light pulse; and the recovery time (τ_{rec}) was defined as the time to recover a 90% of the total response after switching off the light source.

3. Results and discussions

3.1. Electrical and thermal characterisation

The intrinsic resistance of the nanofibers film (R_{sheet}) was first evaluated using the above-described van der Pauw method, the nanofibers films were previously treated at 270 °C to evaporate remains of solvent. Van der Pauw method was repeated at different temperatures, heating up to 270 °C and cooling the sample cyclically. R_{sheet} vs. temperature curves were repeated after completing the first heating cycle (see Supplementary material for more information). In these conditions, a weak negative temperature coefficient behavior was observed since the resistance tends to decrease with increasing temperature. The GANFG sample appears to be more conductive than GANF which is consistent with the material's degree of cristallinity after graphitization. Measurements of the resistance stability of the material at 270 °C vs. time were also carried out (see supplementary material for more information) once the material was previously stabilized at the same temperature (270 °C). Results lead to the conclusion that the electrical properties of the materials do not evolve significantly in a tens of minutes' timescale. In order to characterize the contact resistances R_c, series of 2-probes measurements at different temperatures were performed. In this case, samples were heated up and cooled down cyclically reaching higher temperatures in each cycle. Fig. 1 shows the phenomenological behavior observed in all the samples. It can be clearly seen that the 2-probes resistance values (R_{2P}) display significant hysteretic effects until the treatment temperature reaches the 270 °C. After reaching this temperature, the dependence of the resistance with the temperature is fully repeatable, following a general trend similar to the one observed for the R_{sheet} values.

This results suggest that thermal energies above 270 °C are needed to stabilize the electrical properties of the here-prepared devices and that such treatment must be applied during sufficient time (>2 h).

In order to clarify the contribution of R_c to the total resistance value a series of measurements in fresh samples with multiple contacts with linear arrangement were carried out. This configuration

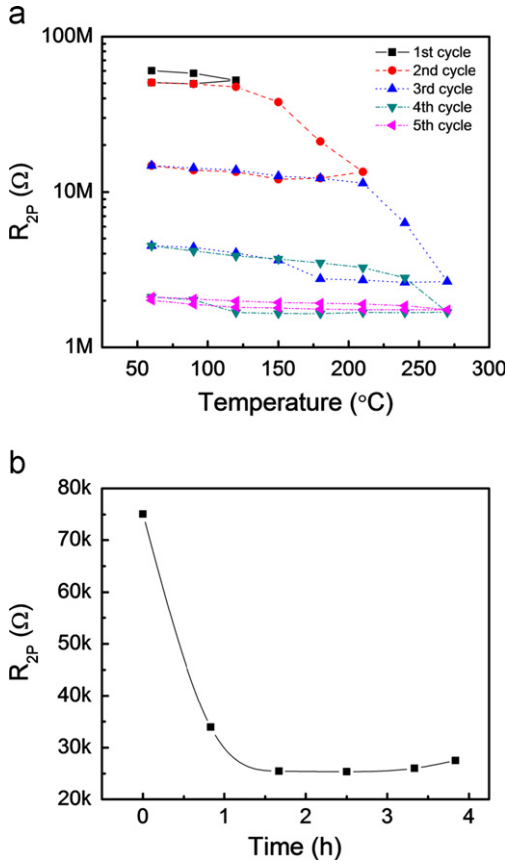

Fig. 1. 2-probes resistance values of GANF deposited by spray. (a) At different temperatures and heating cycles and (b) At 270 °C after the temperature cycles.

allowed us to decouple the R_c values from the fibers film resistance following the previously-described methodology.

As expected, a linear dependence of the total resistance with the interelectrode distance was observed (see supplementary material for more information). The crossing of this linear trend with the *y*-axis allowed us to estimate the R_c values, which were found not negligible, compared to typical values in samples deposited with spray and dropping, respectively. This effect could be minimized by choosing more adequate sintering process of silver electrodes, which can also contribute in this significant contact resistance.

3.2. Gas testing

The preliminary screening of the gas sensing capabilities of the sensors is shown in Fig. 2. In this test the sensor response to a pulse of carbon monoxide, ammonia or humidity (diluted in synthetic air) was checked.

On the one hand, the device barely noticed the CO pulse with a negligible response. In contrast, the sensor response to humidity and ammonia pulses was remarkably larger. For this reason, and from this point on, we focus this first study of the gas sensing properties of GANF and GANFG fibers in the cases of NH_3 and H_2O. On the other hand, we observed that the sensor needs a large time to reach the baseline stabilization, possibly due to room temperature operation, non-functionalized or decorated materials.

In order to study the response of the sensors to ammonia and humidity, two tests for each gas were carried out, which consisted of 5 pulses of decreasing concentration followed by 4 pulses of maximum concentration. This sequence allowed us to study both, the response of the sensor to different concentration and the

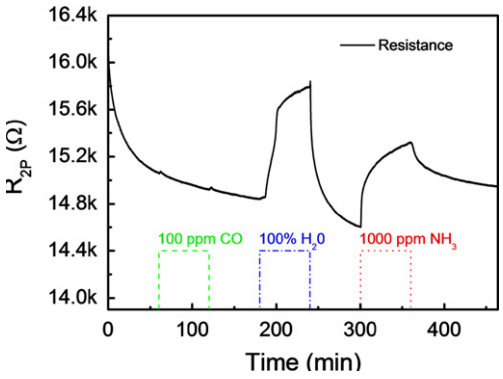

Fig. 2. Resistance change in response to CO, NH_3 and H_2O of a sample of GANF deposited by spray. The water concentration value corresponds to 100% of relative humidity at 25 °C and 1 atm.

repeatability and stability of this signal. As for the response to ammonia, we obtained a linear relationship between the sensor response and the gas concentration. However, this linearity was lost after the first pulses due to a drift of the signal's baseline upon exposure to relatively high concentration of NH_3 (in Fig. 3b).

To clarify the impact of this effect (which seems to be related to the ability of the carbon-based nanofibers to get rid of ammonia adsorbates at room temperature) on the repeatability of the measurements, the sensors were exposed to three pulses of NH_3 at high concentration and three pulses at lower concentration (as shown in Fig. 3c and d). In both cases, the response values were similar within the experimental uncertainty. Therefore, the repeatability of the sensors was not compromised. Moreover, the drift of the signal was only observed in the test with higher concentrations (only first pulse) and no other change in the baseline of the sensor appeared. This suggest that these desorption issues seem to reach some sort of saturation. Thus, from the technological point of view, this effect must be taken into account in order to make meaningful quantitative assessments of the gas presence, especially in the high concentrations range. Finally, the characteristic times of the devices were $\tau_{resp}=35$ min and $\tau_{rec}=45$ min.

As for the response to humidity, we observed a linear behavior with the increasing concentration of water, as in the case of ammonia. The devices had a good repeatability as shown in Fig. 4 b due to the inexistence of the drift seen before. The τ_{resp} and the τ_{rec} values were similar to the response with ammonia gas. Gas tests in GANFG samples were also performed showing properties similar to the one described below for GANF nanofibers. In order to clarify whether the sensor is capable to operate in an ambient atmosphere a final test with two pulses of ammonia without and with humidity was conducted (Fig. 5). The sensor responded similarly in both cases showing only a difference in the baseline, the same result was also found with GANFG nanofibers.

To sum up, the here-studied devices were able to detect NH_3, H_2O and NH_3 in an atmosphere with RH=50%. In NH_3 and H_2O tests linear sensor responses were observed, some drift issues in the baseline arose, especially, for relatively high concentrations. Therefore, the devices performance as a gas sensor was achieved and the gas response found was similar to other studies found in the literature [28,29].

From the point of view of performance, the devices showed a combination of advantages and drawbacks that motivates further studies. On one hand, the use for the first time GANF based on flexible substrates permit its wear-ability and the detection of gases at room temperature which imply low power consumption. On the other hand, a previous thermal treatment could contribute to palliate the baseline drifts [30,31]. Furthermore, the exploration of further strategies to speed up the responses is proposed

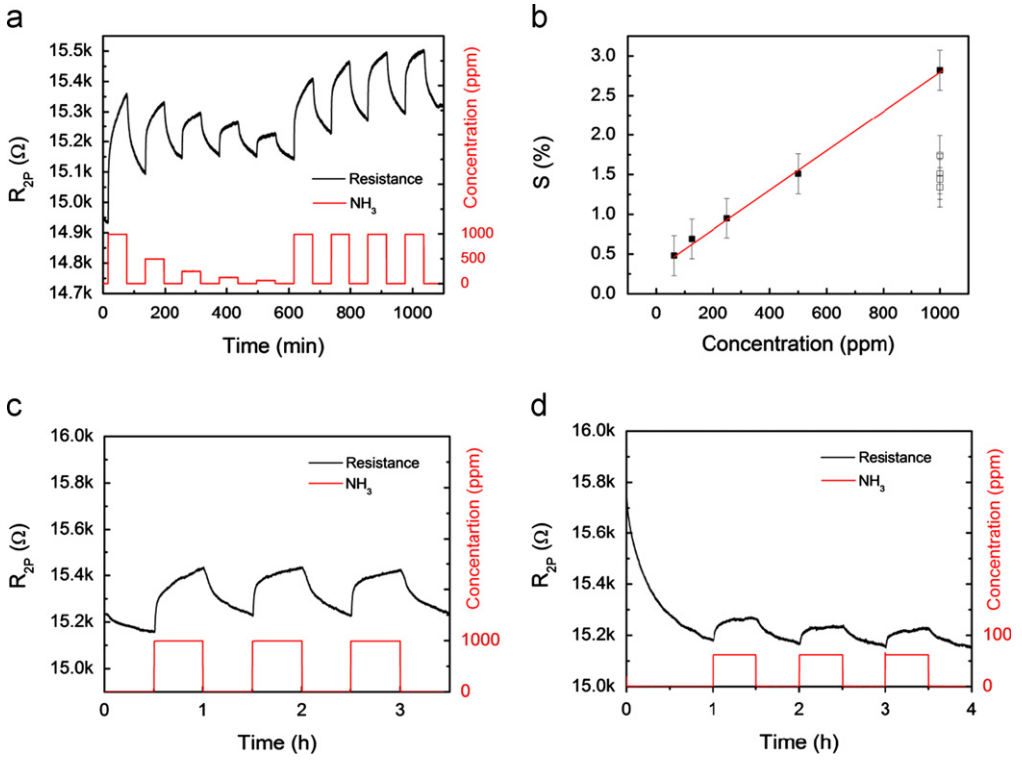

Fig. 3. (a) Resistance change in response to a sequence of NH_3 pulses of a sample of GANF deposited by spray, (b) Response to NH_3 obtained in the gas test experiment shown in (a); the black squares correspond to the first pulses of different concentrations and the white squares to the last pulses with the same concentration, (c) Repeatability test of GANF deposited by spray and exposed to (c) 1000 ppm and (d) 63 ppm of NH_3 diluted in synthetic air.

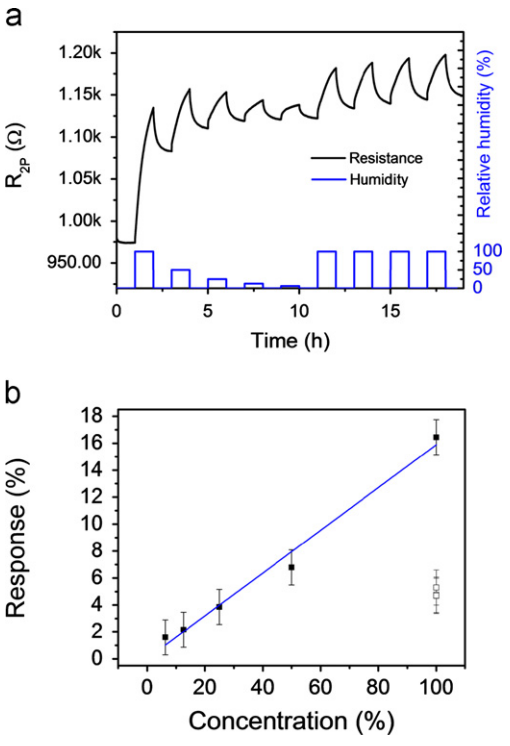

Fig. 4. (a) Resistance change in response to a sequence of humidity pulses of a sample of GANF deposited by spray, (b) Response to H_2O obtained in the gas test experiment shown in (a), the black squares correspond to the first pulses of different concentration and the white squares to the last pulses with the same concentration.

such as temperature and/or illumination [32]. Further studies will consider the decoration of the nanofibers to enhance sensitivity and improves specificity to a wide range of contaminant gases.

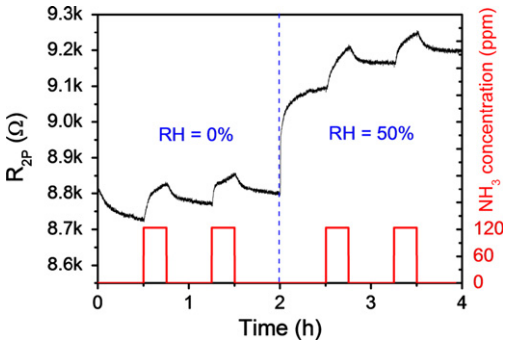

Fig. 5. Comparison of the ammonia sensing response without and with humidity (RH = 50%).

3.3. Mechanical characterization

As mentioned before, Kapton can be easily bended, making the material suitable for future flexible electronics. Two types of measurements were performed: measurements of the resistance at different bending degrees to obtain the gauge factor and repeatability tests applying cyclically the same strain values. The samples resistance varied after deflecting the devices. Fig. 6 shows these bending results. As expected from Eq. (3), the resistance change was proportional to the strain applied, and, depending on the curvature sign, the value of resistance increased or decreased. Surprisingly, a solid shift in the resistance baseline in the two possible directions of deflection was observed. The explanation is a little mechanical perturbation applied in order to create a positive strain in the devices since the samples had not the natural tendency to bend with a positive curvature; this perturbation affected the baseline resistance without altering significantly the general trend. From the point of view of the application as strain sensor, this fact leads to a blind range in the

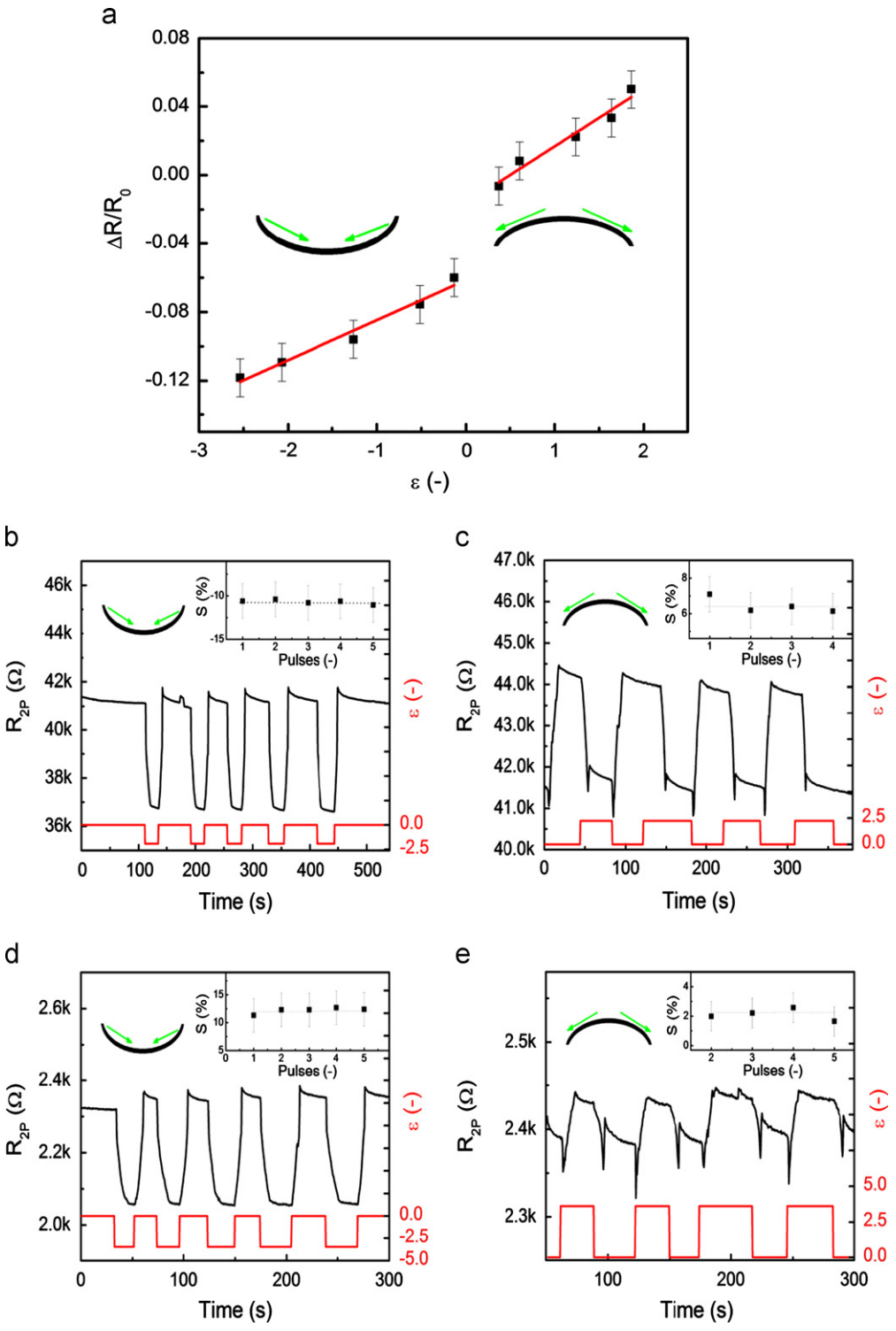

Fig. 6. (a) Plot of the normalized variation of resistance $\Delta R/R_0$ of GANF versus the strain ε caused by bending. Series of equivalent strain pulses applied to GANF with (b) $\varepsilon < 0$ and (c) $\varepsilon > 0$. Series of equivalent pulses applied to GANFG with (d) $\varepsilon < 0$ and (e) $\varepsilon > 0$.

low strain region which could be used as a noise filter in bend-triggered applications.

The gauge factor g of each sample was estimated by fitting each series of data points to the linear law predicted in Eq. (3) (in Table 1). In spite of being quite low compared with conventional gauge sensors (1–200), it has been proven the viability of the carbon nanofibers as a possible material for this type of sensors, these results agree with other studies [33]. As far as repeatability and stability are concerned, the results were very similar for all the pulses in all the tests. It was shown that after bending the sensors recover their baseline, which is crucial to find ways to compensate its influence in sensor responsiveness.

As for the maximum response of the sensors were about 10% at the maximum bending tested, for other applications this

mechanical response could interfere with the performance of the devices with other stimuli. An appropriate package without mechanical flexion could be a simple solution if the response to bending is not desired and flexibility is not required, while preserving the conformability of Kapton.

3.4. Effect of electromagnetic radiation

The response to electromagnetic radiation was also considered, checking the effects of ultraviolet radiation and visible light in the value of resistance of the devices. Previous studies showed how carbon materials display a strong interaction in the region of ultraviolet and visible ranges [34] and that these materials are excellent candidates for photosensors arrays [35].

For UV experiments, the samples were tested with pulses of different intensities to check sensor response. Samples were also exposed to pulses of the same intensity to check repeatability. Fig. 7 shows the results obtained. In both cases, the samples did not fully recover the baseline and there was an enormous resistance change after the first time that the sensors were exposed to the radiation.

Generally speaking, the response of GANFG nanofibers tended to be larger than the response of GANF (in Fig. 7c). Moreover, as mentioned before, the change in the resistance of the sensor is expected to be inversely proportional to the flux of light [30] in moderate illumination conditions. Therefore there should be a linear dependence of the response of the sensor with the intensity of UV light applied as it is shown in Fig. 7. Notice that here we observed this behavior for all the intensities in GANF but there is a data value far away this tendency in the case of GANFG at the maximum intensity. Hence, it seems to suggest that there could be an effect of optical annealing produced in the first pulse.

As for the repeatability, the signals acquired at the same intensity had similar responses and the sensor was capable of recovering the baseline. However, our results indicate that there was an evolution of the response that falls behind the uncertainty of experiment (as shown in Fig. 7d). The τ_{resp} and the τ_{rec} were about 2 min and 10 min for GANF and, respectively about 10 min, 12 min for GANFG.

In visible light experiments, one single light intensity was used due to limitations of the experimental setup. As occurred before with the UV experiments, the signal of the GANFG sample had less noise. The response was also larger with GANFG than with GANF (see supplementary material for more information). As for the response time and recovery time the results were $\tau_{resp}=2.5$ s and $\tau_{rec}=4.1$ s, which is similarly faster than in the case of UV.

Also several voltage vs. current curves were obtained once the signals were stabilized, with and without illumination. Using the expressions of Eqs. (6) and (7), the following relationship can be obtained

$$\left(\frac{R_0}{R}-1\right)\frac{1}{\phi_{ph}}=\frac{\Delta n}{n_0\phi_{ph}}=\frac{\eta\beta\tau}{\alpha^{-1}n_0}\equiv\Sigma \tag{8}$$

where the $\sum$ value only depends on intrinsic properties of the material. The results obtained for $\sum$ are shown in Table 2.

Data clearly show that the nanofibers are more sensitive to radiation in the range of visible light. In addition to this, GANFG had more carriers activated in both wavelength ranges under study. This fact can be directly related to the grade of crystallinity

Table 1
Gauge factor obtained from the linear fitting of data in Fig. 6.

g	$\varepsilon>0$	$\varepsilon<0$
GANF	0.033 ± 0.008	0.023 ± 0.005
GANFG	0.016 ± 0.006	0.027 ± 0.007

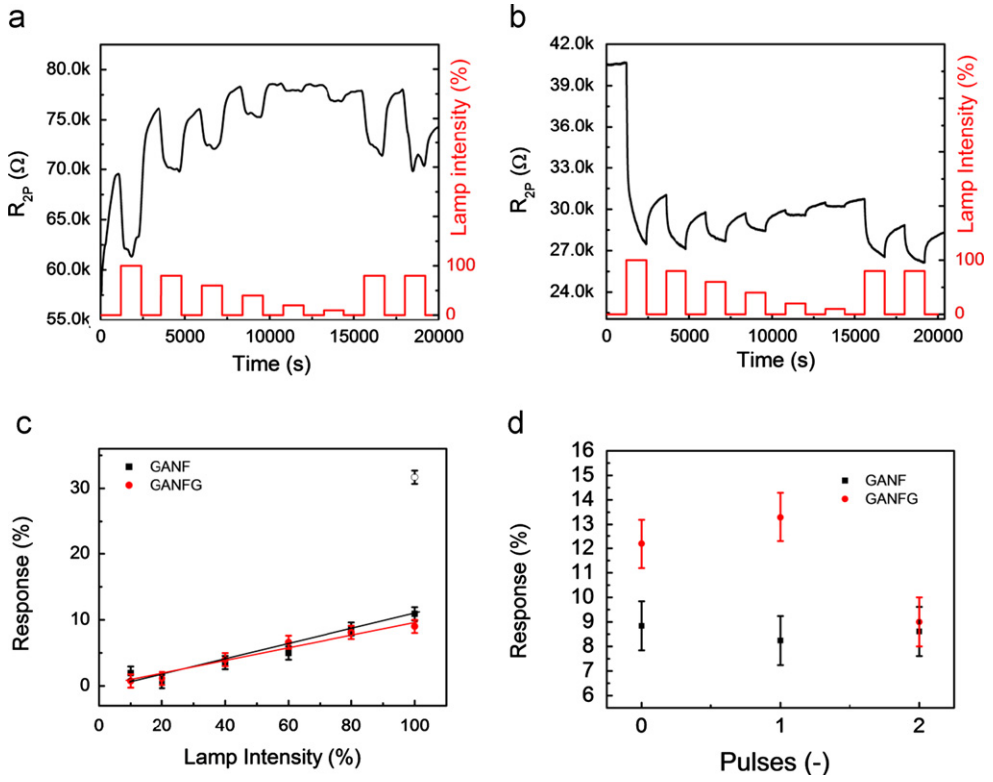

Fig. 7. Resistance variation in (a) GANF and (b) GANFG fibers in response to a sequence of UV light pulses. (c) Response S to increasing intensities of UV radiation of GANF and GANFG. A linear dependence is observed: hollow data point corresponds to the first pulse. (d) Repeatability results obtained for the two samples with UV radiation.

Table 2
Values of Σ.

Σ	UV $(1/(mW/cm^2)\times 10^{-5})$	Visible light $(1/(mW/cm^2)\times 10^{-5})$
GANF	2.2 ± 0.3	23 ± 1
GANFG	9.6 ± 0.1	15 ± 1

of the fibers after graphitization, which is supported by the intrinsic conductivity known by the van der Pauw measurements.

To summarize, GANFG displayed a better response to radiation and both types of nanofibers presented better and faster response and were more repeatable to visible light than UV. With the results obtained it has been demonstrated the viability of the nanofibers as electromagnetic radiation sensors, especially in the range of visible, which makes them suitable for light sensing. It is also important to notice that the effect of radiation cannot be ignored as an interference with other sensing applications.

3.5. Cross-sensitivity effects

The results presented so far show that the sensing material presents a wide range of sensitivities, including mechanical stress and electromagnetic radiation absorption that may interfere with the response to gases. In spite of this drawback, carbon nanofibers are much cheaper than metal oxides or carbon nanotubes [36] and can be operated even at room temperature. These advantages motivate the search for solutions to palliate the cross interference effects. First, GANF and GANFG can be thermally stabilized displaying a repeatable behavior with temperature cycles (Fig. 1) with a maximum variation of the resistance about 10% in case of GANF and 5% with GANFG. This fact makes possible adding a heater operating at stable temperature, slightly above the environment to improve the response and recovery times to gases, as previously reported for other carbon nanostructures [37]. Mechanical stress leads to resistance changes around 7–9% with GANF and 4–11% with GANFG (Fig. 6). These variations are large compared with gas responses. Therefore, the deformation of the substrate must be kept constant during gas detection sequence by means of a suitable packaging whether a strategy to compensate the signal due to the deformation is not taken. Illumination also produces huge variations of the resistance around 1% to 30% (Fig. 7). However, this is the easiest influence to control, just blocking light or UV radiation with an opaque package. Anyhow, all these complexities can also be regarded as an opportunity to integrate multifunctional sensors with specific sensing capabilities in the same platform, using only one single material. In order to optimize the gas sensing operation, on-going studies are devoted to the decoration of the nanofibers with metallic nanoparticles with the aim to improve its response and selectivity.

4. Conclusions

In this work, we demonstrate the feasibility to fabricate low cost and flexible sensors by combining inkjet printing, spray techniques and flexible electronics. The first prototypes were implemented and tested. Gas detection properties at room temperature with good selectivity to the tested gases were achieved. The responsiveness to gases even at room temperature contributes to dramatically moderate the power consumption.

The devices also exhibited sensitivities to temperature, stress/strain/bending and light, demonstrating the multifunctionality of the carbon nanofibers and, allowing this kind of sensors to be used for several applications, as mechanical strain gauges or light detectors. From the point of view of gas sensing, cross-sensitivity issues are discussed, and methods to prevent this cross-interference are proposed. All these results open the door to a next generation of gas sensors with new sensing features.

Acknowledgements

This work is carried out in the framework of INFINITEX project (Investigacio´n de Nuevas Funcionalidades e Inteligencia Implementadas en Textiles), financed by Centro para el Desarrollo Tecnológico Industrial from Spanish Science and Innovation Ministry. The authors thankfully acknowledge the contribution of the technological center CETEMMSA in the integration of the devices in textile garments.

Some of the research leading to these results was also funded by the Project VALTEC09-2-0053 (ACC1Ó, Generalitat de Catalunya; cofunded by FEDER in the framework of the Programa Operatiu de Catalunya).

Mikel Martinez de Marigorta has been funded by grant number 2010 TEM 48 from the Generalitat of Catalonia.

Albert Cirera acknowledges financial support from ICREA Academia program.

Appendix A. Supporting information

Supplementary data associated with this article can be found in the online version at http://dx.doi.org/10.1016/j.talanta.2013.01.022.

References

[1] K. Parikh, K. Cattanach, R. Rao, D.-S. Suh, A. Wu, S.K. Manohar, Sens. Actuators, B 113 (2006) 55–63.
[2] K. Mitsubayashi, Y. Wakabayashi, D. Murotomi, T. Yamada, T. Kawase, S. Iwagaki, I. Karube, Sens. Actuators, B 95 (2003) 373–377.
[3] P.-G. Su, C.-T. Lee, C.-Y. Chou, K.-H. Cheng, Y.-S. Chuang, Sens. Actuators, B 139 (2009) 488–493.
[4] R. Gadh, G. Roussous, K. Michael, G.Q. Huang, B.S. Prabhu, P. Chu, Proc. IEEE 98 (2010) 1546–1549.
[5] G.H. Gelinck, E. Huitema, E. van Veenendaal, L. Cantatore, J.B.P.H. Schrinjnemakers, T.C.T. van der Putten, M. Gaeuns, J.B. Beenhakkers, B.H. Giesbers, E.J. Huisman, E.M. Meijer, F.J. Benito, A.W. Touwslager, B.J.E. Marsman, Rens van, M. Dago, Leeuw de, Nat. Mater. 3 (2004) 106–110.
[6] L. Zhou, A. Wanga, A.C. Wu, J. Sun, S. Park, T.N. Jackson, Appl. Phys. Lett. 88 (2006) 083502.
[7] B. Crone, A. Dodabalapur, A. Gelperin, L. Torsi, H.E. Katz, A.J. Lovinger, Z. Bao, Appl. Phys. Lett. 78 (2001) 2229–2231.
[8] C.W. Sele, T. Von Werne, R.H. Friend, H. Sirringhaus, Adv. Mater. 17 (2005) 997–1001.
[9] B.J. De Gans, P.C. Duineveld, U.S. Schubert, Adv. Mater. 16 (2004) 203–213.
[10] H. Sirringhaus, T. Kawase, R.H. Friend, T. Shimoda, E.P. Woo, Science 290 (2000) 2123–2326.
[11] T. Kawase, H. Sirringhaus, R.H. Friend, T. Shimoda, Adv. Mater. 13 (2001) 1601–1605.
[12] L. Torsi, G.M. Farinol, F. Marinelli, M.C. Tanese, O.H. Omar, L. Valli, F. Babudri, F. Palmisano, P.G. Zambonin, F. Naso, Nat. Mater. 7 (2008) 412–417.
[13] N.B. Cho, T.H. Lim, Y.M. Jeon, M.S. Gong, Sens. Actuators, B 130 (2008) 594–598.
[14] K. Crowley, A. Morrin, A. Hernandez, E. O'Malley, P.G. Whitten, G.G. Wallace, M.R. Smyth, A.J. Killard, Talanta 77 (2008) 710–717.
[15] P.G. Su, C.T. Lee, C.C. Yi, Talanta 80 (2009) 763–769.
[16] B. Weng, R.L. Shepherd, K. Crowley, A.J. Killard, G.G. Wallace, Analyst 135 (2010) 2779–2798.
[17] M.F. Mabrook, C. Pearson, M.C. Petty, IEEE Sens. J. 6 (2006) 1435–1444.
[18] T. Mayr, T. Abel, B. Enko, S. Borisv, C. Konrad, S. Kostler, B. Lamprecht, S. Sax, E.J.W. List, L. Klimant, Analyst 134 (2009) 1544–1547.
[19] V. Subramanian, P.C. Chang, J.B. Lee, S.E. Molesa, S.K. Volkman, IEEE Trans. Compon. Packag. Manuf. Technol. Part A: 28 (2005) 742–747.
[20] I. Jiménez, A. Cirera, J. Folch, A. Cornet, J.R. Morante, Sens. Actuators, B 78 (2001) 78–82.
[21] I. Jiménez, A. Cirera, A. Cornet, J.R. Morante, I. Gracia, C. Cané, Sens. Actuators, B 84 (2002) 78–82.

[22] DuPontTM Kapton® HN polyimide film [online], [consulted on September 15th, 2011], Available at: 〈http://www.2.dupont.com/Kapton/en_US/assets/downloads/pdf/HN_datasheet.pdf〉.
[23] L.J. Van der Pauw, Philips Res. Rep. 13 (1958) 1–9.
[24] L.J. Van der Pauw, Philips Tech. Rev. 20 (1958) 220–224.
[25] M. Weisenberger, I. Martín-Gullon, J. Vera-Agullo, H. Varela-Rizo, C. Merino, R. Andrews, D. Qian, T. Rantell, Carbon 47 (2009) 2211–2218.
[26] S.M. Sze, K. Ng, Physics of Semiconductor Devices, third ed., John Wiley & Sons, Hoboken, 2007.
[27] J.D. Prades, R. Jimenez-Díaz, F. Hernandez-Ramirez, L. Fernandez-Romero, T. Andreu, A. Cirera, A. Romano-Rodriguez, A. Cornet, J.R. Morante, S. Barth, S. Mathur, J. Phys. Chem. C 112 (2008) 14639–14644.
[28] M. Gautam, A.H. Jayatissa, Mater. Sci. Eng., C 31 (2011) 1405–1411.
[29] Y. Battie, O. Ducloux, P. Thobois, N. Dorval, J.S. Lauret, B. Attal-Trétout, A. Loiseau, Carbon 49 (2011) 3544–3552.
[30] M. Roth, R. Hartinger, R. Faul, H.-E. Endres, Sens. Actuators, B 35-36 (1996) 358–362.
[31] G. Korotcenkov, B.K. Cho, Sens. Actuators, B 156 (2011) 527–538.
[32] G. Lu, L.E. Ocola, J. Chen, Nat. Nanotechnol. 20 (2009) 445502–445511.
[33] F.-Y. Chang, R.-H. Wang, H. Yang, Y.-H. Lin, T.-M. Chen, S.-J. Huang, Thin Solid Films 518 (2010) 7343–7347.
[34] Y. Zhang, S. Iijima, Phys. Rev. Lett. 82 (1999) 3472–3475.
[35] C.-M. Lin, W. Fang, Nat. Nanotechnol. 20 (2009) 4665502–4665510.
[36] I. Kang, Y.Y. Heung, J.H. Kim, J.W. Lee, R. Gollapudi, S. Subramaniam, S. Narasimhadevara, D. Hurd, G.R. Kirikera, V. Shanov, M.J. Schulz, D. Shi, J. Boerio, S. Mall, M. Ruggles-Wren, Composites Part B 37 (2006) 382–394.
[37] J.D. Fowler, M.J. Allen, V.C. Tung, Y. Yang, R.B. Kaner, B.H. Weiller, ACS Nano 3 (2009) 301–306.